JMES The International Journal of
Mechanical Engineering and Sciences
https://journal.its.ac.id/index.php/jmes/index
e-ISSN 2580-7471

Thermal Performance Analysis of an Integrated Solar Still and Solar Thermal Collector System

Ivana Dzakiyyah Ramadhani, Ridho Hantoro*, Erna Septyaningrum

Department of Physics Engineering, ITS, Sukolilo, Surabaya, 60111, Indonesia

Received: 17 June 2026, Revised: 29 June 2026, Accepted: 30 June 2026

Abstract

Solar still desalination is a simple and low-energy technology for producing freshwater from saline water, however, its practical application is still limited by low evaporation rate and distillate productivity. This study analytically evaluates the thermal performance of a double-slope solar still integrated with a flat-plate solar thermal collector. The objective is focused on assessing the effect of collector integration on useful heat gain, thermal efficiency, and water productivity. The system was modelled using a thermal resistance network under quasi-steady hourly conditions from 06:00 to 18:00 WIB. The analytical model accounts for conduction, convection, and radiation heat transfer, along with the evaporation and condensation processes. The results show that adding the solar thermal collector significantly improves the thermal performance of the solar still. The daily average thermal efficiency increased from 10.22% to 20.44% during the dry season and from 7.69% to 15.39% during the rainy season. Daily productivity also increased from 0.86 to 1.10 L/m^2/day in the dry season and from 0.51 to 0.96 L/m^2/day in the rainy season. Therefore, integrating a solar thermal collector enhances solar still performance by increasing thermal energy supply to the evaporation chamber.

Keywords: Desalination, Heat Transfer, Solar Still, Solar Thermal Collector, Thermal Efficiency.

1. Introduction

Water is an essential resource for sustaining life and supporting domestic, agricultural, and industrial activities. Approximately 97.5% of the water on Earth is saline, meaning that only 2.5% of the freshwater suitable for human use is available [1]. The United Nations Report states that changes in consumption patterns, particularly eating habits, and economic and social development are the main causes of the annual growth of less than 1% in freshwater use worldwide [2]. Freshwater consumption for agriculture is around 70%, industry around 20%, and domestic use around 10%, which are the main areas where freshwater demand is increasing [3]. More than 780 million people worldwide today are affected by water scarcity [4]. Based on data from the Central Bureau of Statistics (2024), only 92.64% of national households have access to adequate drinking water, with 96 in urban areas, 83.91% in rural areas, and only 11.90% meeting the safe standards of Minister of Health Regulation No. 32 of 2017. Therefore, desalination has become an important alternative for addressing freshwater scarcity, particularly in coastal and arid regions.

Desalination is the process of purifying freshwater from brackish or saltwater into clean water [5, 6]. Thermal desalination and membrane desalination are the two desalination techniques used to purify salt water [2, 3]. The membrane method predominates in the desalination process, making up 69–73% of all systems installed globally, whereas the thermal approach makes up only roughly 27% [7, 8]. Desalination requires energy to remove salts and minerals from seawater, thereby converting it into freshwater [9].

Thermal desalination and membrane desalination are the two primary types of desalination techniques used to purify saltwater. Membrane-based desalination procedures account for 69–73% of all deployed systems globally, while thermal techniques make up about 27%. Through cyclic evaporation and condensation, thermal desalination systems use external heat to transform saltwater into drinkable water. The most popular kinds are mechanical vapor compression (MVC), thermal vapor compression (TVC), multi-effect distillation (MED), and multi-stage flash desalination (MSF). In contrast, membrane desalination uses permeable membranes to remove salts from saline water without causing a phase shift. These pressure-driven procedures are frequently called electrodialysis and reverse osmosis (RO) [10].

A solar still is one of the desalination processes that uses solar energy as the main energy source to support the seawater desalination process [8, 9]. Solar energy is a renewable energy source that is widely used for water desalination [8, 11]. In the hydrological cycle, water vapor

*Corresponding author. Email: hantoro@its.ac.id

Table 1. Main system specifications and analytical variables.

Item	Description
Solar still type	Double-slope basin solar still
Solar still basin area	1×1 m^2
Solar thermal collector type	Flat-plate solar air collector
Solar thermal collector area	1×0.6 m^2
Operating period	06:00–18:00 WIB
Compared configurations	SS, STC, and integrated SS+STC
Main outputs	Useful heat, thermal efficiency, temperature response, productivity

Table 2. Temperature measurement points in the experimental setup.

Point	Item	Description	System
1	Glass cover temperature, (T_c)	Surface of solar still glass cover	SS
2	Basin water temperature, (T_w)	Basin water inside solar still	SS
3	Absorber plate temperature, (T_p)	Absorber/basin plate surface	SS
4	Collector glass cover temperature, (T_c)	Surface of STC glass cover	STC
5	Collector absorber plate temperature, (T_p)	Absorber plate surface of STC	STC

is generated by heating seawater using solar radiation, followed by vapor condensation, which ultimately produces condensate that is subsequently collected as product water [3]. The main advantages of a solar still are its low operating cost and the utilization of clean, emission-free energy; however, its major limitation is low productivity [2]. A research study shows that under high irradiation conditions, the passive distillation output of conventional solar stills is only about 4–6 L/m^2 per day, which is a clean water volume that is far from the needs of rural households [12]. Research by Hassan (2020) indicates that the addition of an external collector, in the form of a parabolic trough collector, can significantly enhance the performance of a solar still. A double-slope solar still + PTC system produces productivity of 8.53 kg/m^2/day in summer and 4.03 kg/m^2/day in winter [13, 14].

This demonstrates that additional heat supply from the collector can increase the water temperature, enlarge the water-glass temperature difference, and increase the evaporation rate. Therefore, the development of technologies is needed to improve the efficiency of this system before it can be widely implemented. One innovative approach is to integrate a solar still with a solar thermal collector. The development of this technology is carried out by using a solar still system integrated with a solar thermal collector to increase the efficiency and productivity of desalinated water. This study compares three configurations: a conventional solar still (SS), a standalone solar thermal collector (STC), and an integrated solar still–solar thermal collector system (SS+STC).

Integrating a solar still with a solar thermal collector is a promising strategy to increase heat input, enhance basin water temperature, and improve distillate productivity. Therefore, this study compares three configurations: a conventional solar still (SS), a solar thermal collector (STC), and an integrated solar still–solar thermal collector system (SS+STC). The system performance was evaluated using useful heat gain, thermal efficiency, evaporation rate, and freshwater productivity under dry and rainy season conditions. The novelty of this study lies in the analytical comparison of SS, STC, and SS+STC configurations under seasonal climatic conditions using validated temperature data and integrated thermal performance indicators.

2. Theoretical method

2.1. Weather Data and Location

This study was conducted using NASA POWER data from January to December 2025, covering the period from 06:00 to 18:00 Western Indonesian Time (WIB), to obtain solar radiation intensity and wind speed data. The research location for the solar thermal collector and solar still systems was positioned at a latitude of 7.276°S and a longitude of 112.793°E. The study was carried out using

Figure 1. Configuration of the Solar Still (SS) and Solar Thermal Collector (STC) Systems.

Figure 2. Measurement points of temperature in the experimental setup: (1) glass cover temperature of the solar still, (2) basin water temperature, (3) absorber plate temperature of the solar still, (4) glass cover temperature of the solar thermal collector, and (5) absorber plate temperature of the solar thermal collector.

three system configurations: a solar still (SS), a solar thermal collector (STC), and an integrated solar still and solar thermal collector system (SS+STC). The performance of the solar distillation systems was evaluated based on several research variables, including useful energy gain (Q_u) as a function of time, hourly thermal efficiency as a function of time, hourly evaporation rate as a function of time, and hourly freshwater productivity variations during the dry and rainy seasons. In this study, the dry season was classified as occurring from April to October, while the rainy season was classified as occurring from November to March [15].

2.2. System Configuration

The analyzed system consisted of a conventional solar still (SS), a solar thermal collector (STC), and an integrated configuration in which heated air from the solar collector received additional thermal energy from the collector. The SS acted as the evaporation and condensation chamber. Saline water was placed in a blackened basin, solar radiation penetrated the glass cover, and vapor condensed on the cooler inner glass surface. The STC acted as an auxiliary solar air heater. Solar radiation was absorbed by the collector absorber plate, transferred to the air stream through convection, and transported toward the solar still as sensible heat.

The experiment was conducted in the parking area of the Department of Engineering Physics, ITS. Data collection was carried out continuously at 60-minute measurement intervals during the daily testing period, from morning to afternoon, specifically from 09:00 to 16:00 WIB, to capture variations in solar radiation conditions. All collected data were then tabulated and analyzed to evaluate the effect of roof design variations on temperature distribution, heating effectiveness, and distillate water productivity in the solar still system. The testing was conducted in the Engineering Physics parking area for 8 hours, from 09:00 to 16:00 WIB, under solar radiation intensity conditions that supported the heating and evaporation processes of seawater.

The principal dimensions and operating variables used in the analytical model are compiled in Table 1. The solar still basin area was 1×1 m^2, while the solar thermal collector area was 1×0.6 m^2. The system was evaluated from 06:00 to 18:00 WIB using hourly solar radiation and ambient temperature data. The model assumed quasi-steady behavior at each hourly interval, one-dimensional heat transfer through the main thermal path, constant representative thermophysical properties over each interval, and heat loss to the environment through convection and radiation. Figure 1 illustrates the thermal interaction between the STC and the solar still considered in this work.

The experimental setup was equipped with temperature measuring instruments to monitor the thermal response of the solar still (SS) and solar thermal collector (STC). In the solar still system, three temperature measurement points were used: the temperature of the glass cover, the water in the basin, and the temperature of the absorber plate. In order to assess the condensation surface temperature, the glass cover temperature was measured on the solar still's surface. The basin water temperature was measured inside the basin to represent the water temperature during the heating and evaporation processes. The absorber plate temperature was measured on the basin absorber surface to determine the heat absorption characteristics of the solar still.

Temperature measurements were conducted at five main points: the glass cover, basin water, and absorber plate of the solar still, as well as the glass cover and absorber plate of the solar thermal collector. The temperature measuring instruments had an accuracy of approximately ± 0.5°C. Solar radiation intensity was measured using a pyranometer placed near the experimental setup in an unshaded area, with an accuracy of approximately $\pm 5\%$. Distillate productivity was measured using a measuring cylinder based on its scale resolution. All measurements were recorded at 60-minute intervals during the experimental period.

In the solar thermal collector system, two temperature measurement points were used, namely the glass cover temperature and absorber plate temperature. The glass cover temperature of the STC was measured on the collector cover surface, while the absorber plate temperature was measured on the collector absorber surface to evaluate the heat absorption process in the collector. Solar radiation intensity was measured using a pyranometer placed near the experimental setup in an open area without shading. The pyranometer was positioned to represent the incident solar radiation received by both the solar still and solar thermal collector during the experiment.

2.3. Analytical Model

The analytical model was developed using a thermal resistance network. The network approach expresses each heat-transfer mechanism as a thermal resistance and enables the useful heat transfer rate to be estimated from the driving temperature difference. In the solar thermal collector, the main processes include solar absorption by the absorber plate, conduction through solid components, convection from the absorber surface to air, and heat loss from the top, bottom, and side surfaces. In the solar still, the main processes include solar absorption by the basin water and basin plate, evaporative heat transfer from water to moist air, radiative exchange between water and glass, convective heat transfer inside the still, conduction through the glass and basin, and external convection and radiation from the glass cover to the ambient air.

The temperature differential between the basin water and the glass cover primarily controls the evaporation and condensation processes in the solar still. The water temperature and saturation vapor pressure rise as a result of the basin water absorbing solar energy and extra heat from the STC. When the glass temperature drops below the vapor temperature, the produced vapor subsequently condenses on the inner glass cover surface. Therefore, the heat transfer from water to glass includes convective, radiative, and evaporative components. The latent heat of vaporization and the evaporative heat transfer coefficient were used to compute the evaporation and condensation rates using Equation (1).

$$h_{e,w-c} = 16.273 \times 10^{-3}\, h_{c,w-c} \left(\frac{P_w - P_c}{T_w - T_c} \right) \tag{1}$$

Where, $h_{e,w-c}$ is the evaporative heat transfer coefficient between basin water and glass cover (W/m^{2}K), $h_{c,w-c}$ is the convective heat transfer coefficient between basin water and glass cover (W/m^{2}K), P_w is the saturated vapor pressure at basin water temperature (Pa), P_c is the saturated vapor pressure at glass cover temperature (Pa), T_w is the basin water temperature (°C), and T_c is the glass cover temperature (°C). Evaporative heat transfer rate is calculated using Equation (2).

$$q_{r,w-c} = h_{e,w-c}\,(T_w - T_c) \tag{2}$$

Therefore, $q_{r,w-c}$ is the radiative heat transfer rate from basin water to glass cover (W/m^2), and $h_{c,w-c}$ is the convective heat transfer coefficient between basin water and glass cover (W/m^{2}K). Radiative heat transfer coefficient between basin water and glass cover is calculated using Equation (3).

$$h_{r,w-c} = \varepsilon_{\text{eff}}\sigma \left[(T_w + 273.15)^2 + (T_c + 273.15)^2 \right] \times \left[(T_w + 273.15) + (T_c + 273.15) \right] \tag{3}$$

Where, $h_{r,w-c}$ is the radiative heat transfer coefficient between basin water and glass cover (W/m^{2}K). Effective emissivity is calculated using Equation (4).

$$\varepsilon_{\text{eff}} = \left(\frac{1}{\varepsilon_w} + \frac{1}{\varepsilon_c} - 1 \right)^{-1} \tag{4}$$

Where, ε_{eff} is the effective emissivity between basin water and glass cover, ε_w is the emissivity of basin water, and ε_c is the emissivity of the glass cover. Radiative heat transfer rate is calculated using Equation (5).

$$q_{r,w-c} = h_{r,w-c}\,(T_w - T_c) \tag{5}$$

Where, $q_{r,w-c}$ is the radiative heat transfer rate from basin water to glass cover (W/m^2), $h_{r,w-c}$ is the radiative heat transfer coefficient between basin water and glass cover (W/m^{2}K). Total heat transfer from basin water to glass cover is calculated using Equation (6).

$$q_{w-c} = (h_{c,w-c} + h_{r,w-c} + h_{e,w-c})\,(T_w - T_c) \tag{6}$$

Where, $q_{r,w-c}$ is the total heat transfer rate from basin water to glass cover (W/m^2), $h_{c,w-c}$ is the convective heat transfer coefficient between basin water and glass cover (W/m^{2}K). Condensation rate is calculated using Equation (7).

$$\dot{m}_{\text{cond}} = \frac{h_{e,w-c} A_c\,(T_w - T_c)}{h_{fg}} \tag{7}$$

Where, $\dot{m}_{\text{cond}}$ is the condensation rate of water vapor (kg/s), $h_{e,w-c}$ is the evaporative heat transfer coefficient between basin water and glass cover (W/m^{2}K), A_c is the glass cover area or condensation surface area (m^2), and h_{fg} is the latent heat of vaporization of water (J/kg). The water-glass energy balance is calculated using Equation (8).

$$\alpha_\omega \tau_g I + \frac{Q_u}{A_c} = (h_{c,w-c} + h_{r,w-c} + h_{e,w-c})\,(T_w - T_c) + U_b(T_w - T_c) \tag{8}$$

Where, α_w is the absorptivity of basin water, τ_g is the transmittance of the glass cover, I is the solar radiation intensity (W/m^2), Q_u is the useful heat supplied to the system (W), A_c is the useful heat supplied to the system (W), and U_b is the bottom heat loss coefficient (W/m^{2}K).

Solar radiation energy (S) received by the corrugated absorber plate is partially converted into useful energy (Q_u), while the remaining portion is lost as thermal losses through the top (U_t) and bottom (U_b) parts of the collector. The heat transfer coefficient through the front surface of the collector (U_t) can be expressed based on the thermal resistance approach using Equation (9).

$$U_t = \left[\frac{1}{h_{c,p-c} + h_{r,p-c}} + \frac{1}{h_w + h_{r,c-a}} \right]^{-1} \tag{9}$$

Where, U_t is the overall top heat loss coefficient of the collector, $h_{c,p-c}$ is the convective heat transfer coefficient between the absorber plate and the cover glass, $h_{r,p-c}$ is the radiative heat transfer coefficient between the absorber plate and the cover glass, $h_{r,c-a}$ is the radiative heat transfer coefficient between the cover glass and the ambient air [16].

Energy loss through the bottom part of the collector occurs due to heat conduction through the insulation layer, followed by heat dissipation to the surrounding air through convection and thermal radiation. The bottom heat loss coefficient of the collector is expressed in Equation (10).

$$U_b = \frac{k}{L} \tag{10}$$

Where, k is the thermal conductivity of the insulation material (W/m·K), L is the thickness of the insulation layer beneath the collector (m) [16]. Therefore, the overall heat loss coefficient can be calculated using Equation (11).

$$U_L = U_t + U_b \tag{11}$$

Where, U_L is the total heat loss coefficient (W/m^{2}K), U_t is the top heat loss coefficient of the collector (W/m^{2}K), and U_b is the bottom heat loss coefficient of the collector (W/m^{2}K) (Beckman and Blair, 2020). Air, as the working fluid in this system, absorbs heat along its flow path inside the collector. The absorbed solar radiation is calculated using Equation (12).

$$S = \tau_{cg}\alpha_{\text{abs}}I_T \tag{12}$$

Where, S is the absorbed solar radiation per unit area (W/m^2), τ_{cg} is the transmittance of the cover glass, α_{abs} is the absorptivity of the absorber plate, and I_T is the solar radiation intensity (W/m^2) [16].

The useful heat gain of the solar thermal collector under steady-state conditions can be estimated from the difference between the absorbed solar radiation and the thermal losses, as expressed in Equation (13).

$$Q_u = A_C\left[S - U_L\left(T_{pm} - T_a\right)\right] \tag{13}$$

Where, Q_u is the useful heat gain of the collector (W), A_C is the collector area (m^2), S is the absorbed solar radiation per unit area (W/m^2), U_L is the total heat loss coefficient (W/m^2), T_{pm} is the mean absorber plate temperature (°C or K), and T_a is the ambient air temperature (°C or K) [16]. The thermal efficiency of the solar thermal collector is calculated using Equation (14).

$$\eta = \frac{Q_u}{I_T A_C} \tag{14}$$

Where, η is the thermal efficiency of the solar thermal collector, Q_u is the useful heat gain absorbed by the air (W), I_T is the solar radiation intensity (W/m^2), and A_C is the collector area (m^2) [16]. The evaporation rate generated by the useful heat input can be calculated using Equation (15).

$$\dot{m}_{\text{evap}} = \frac{\dot{Q}_u}{h_{fg}} \tag{15}$$

Where, $\dot{m}_{\text{evap}}$ is the evaporation rate (kg/s), Q_u is the useful heat input (W), and h_{fg} is the latent heat of vaporization (J/kg) [8]. The daily amount of condensed water, or daily productivity, can be estimated using Equation (16).

$$\dot{m}_d = \dot{m}_{\text{evap}} \times 3600 \text{ s/hour}\times \tag{16}$$

Where, m_d is the daily distillate mass (kg/day), $\dot{m}_{\text{evap}}$ is the evaporation rate (kg/s), and t is the operating duration (h/day). In this study, the operating duration was taken as 12 h/day. The volumetric productivity can then be obtained using Equation (17).

$$V = \frac{\dot{m}_d}{\rho} \tag{17}$$

Where, $\forall$ is the daily volumetric productivity (m^2/day) or (L/day), m_d is the daily distillate mass (kg/day), and A_b is the basin area (m^2) [17].

2.4. Model Validation and Performance Indicators

The analytical temperature results were validated against experimental temperature data for the absorber plate, glass cover, and basin water. The absorber plate and glass cover were compared for both the SS and STC configurations, while the basin water temperature was evaluated for the solar still. The validation was performed using root mean square error (RMSE), mean absolute error (MAE), mean absolute percentage error (MAPE), and the coefficient of determination (R^2).

The validation was performed using experimental data collected at 60-minute intervals during the testing period. For each daily experiment, nine data points were obtained from 09:00 to 16:00 WIB. The analytical model was validated using absorber plate temperature, glass cover temperature, and basin water temperature. Productivity and thermal efficiency were then evaluated as derived performance indicators based on the validated thermal response. The temperature sensors had an uncertainty of ± 0.5°C, while the pyranometer had an uncertainty of approximately $\pm 5\%$. The uncertainty of distillate productivity was associated with the resolution of the measuring cylinder used to collect condensate. The validation metrics used in this study were RMSE, MAE, MAPE, and the coefficient of determination R^2.

These metrics indicate the deviation between analytical and experimental values as well as the ability of the model to follow the measured temperature trend. After validation, the effect of collector integration was evaluated using three main performance indicators: useful heat response, daily average thermal efficiency, and daily distillate productivity. The comparison emphasized the difference between the passive SS and the integrated SS+STC system under dry season and rainy season conditions.

3. Results and Discussion

3.1. Model Validation

The validation results indicate that the analytical model can reasonably represent the measured thermal response of the system. Table 3 shows that the MAPE values for all evaluated temperatures were below 3.37%. The absorber plate temperature of the SS produced an RMSE of 1.354 and an R^2 of 0.9567, while the STC absorber plate temperature produced an RMSE of 1.683 and an R^2 of 0.9640. The glass temperature also showed acceptable agreement, with R^2 values of 0.9081 for SS and 0.9299 for STC. The basin water temperature had a slightly lower R^2 of 0.8629, which is physically reasonable because water temperature changes are influenced by heat storage, evaporation, and transient environmental effects.

The comparison between the experimental and analytical glass cover temperatures (T_c) in the solar still (SS) system, with values of 40.87°C and 40.52°C, respectively. The validation results showed an RMSE of 1.133, MAE of 0.941, MAPE of 2.32%, and R^2 of 0.908. In the solar thermal collector (STC) system, the experimental and analytical values of (T_c) were 61.76°C and 61.99°C, respectively, with an RMSE of 1.568, MAE of 1.358, MAPE of 2.24%, and R^2 of 0.929. Meanwhile, the validation results for the basin water temperature (T_w) in the SS system showed that the experimental and analytical values were 46.12°C and 44.60°C, respectively. The corresponding statistical indicators were an RMSE of 1.632, MAE of 1.506, MAPE of 3.36%, and R^2 of 0.862. These results show that there was not much of a difference between the analytical and experimental calculations. Therefore, the analytical model can be used to predict and validate the experimental results, particularly for the glass cover temperature (T_c).

The agreement between the experimental and analytical data indicates that the model is capable of predicting the thermal response of the system with acceptable accuracy. Nevertheless, slight discrepancies between the experimental and analytical results were still observed because the analytical model was developed based on several assumptions, including quasi-steady-state conditions, one-dimensional heat flow, and constant heat transfer coefficients at each time interval. Under actual operating conditions, the convective heat transfer coefficient may vary depending on wind velocity, system orientation, surface temperature, and surrounding environmental conditions.

Therefore, the validation results confirm that the analytical model can be applied as an appropriate ap-

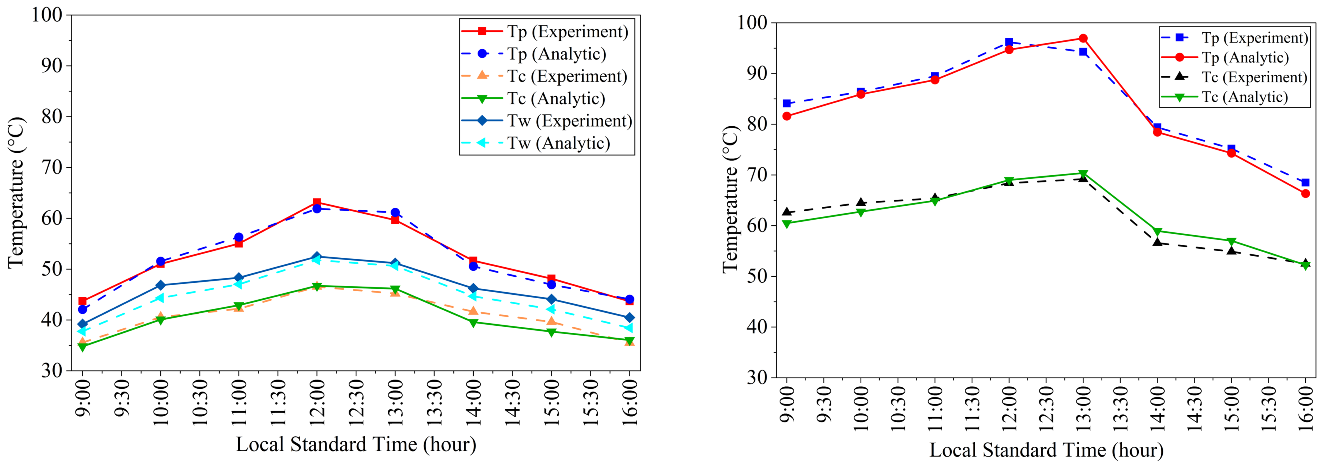

(a) SS System.

(b) STC System.

Figure 3. Analytical and Experimental Validation of Absorber Plate Temperature, Glass Cover Temperature, and Water Temperature with Time: (a) Solar Still System and (b) Solar Thermal Collector.

Table 3. Validation metrics of analytical and experimental temperature data.

Parameter	System	RMSE	MAE	MAPE (%)	R^2
Absorber plate temperature	SS	1.354	1.245	2.408	0.9567
	STC	1.683	1.484	1.782	0.9640
Glass temperature	SS	1.133	0.941	2.327	0.9081
	STC	1.568	1.358	2.242	0.9299
Basin water temperature	SS	1.632	1.506	3.369	0.8629

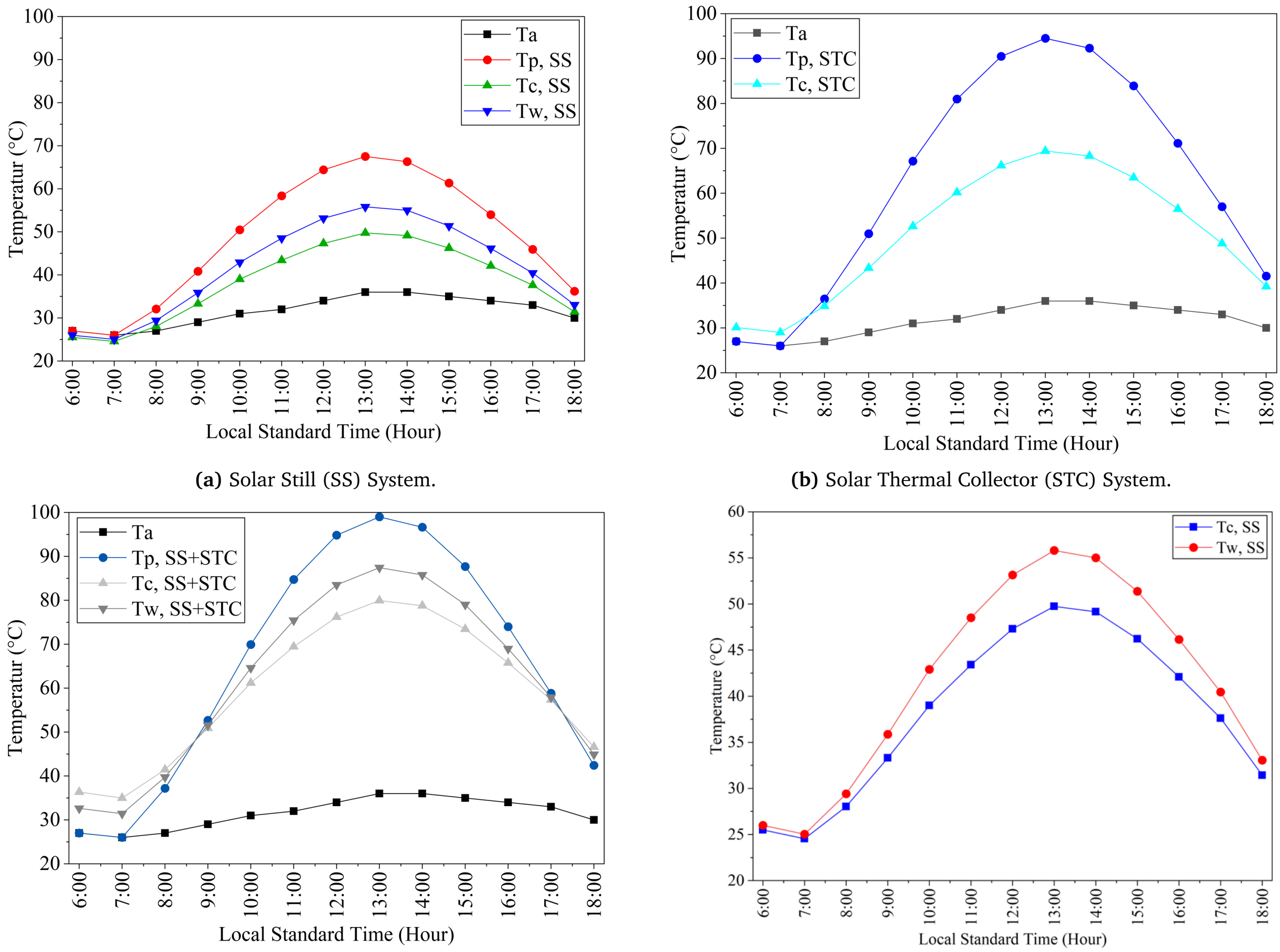

(a) Solar Still (SS) System.

(b) Solar Thermal Collector (STC) System.

(c) SS+STC System.

(d) Variation of ΔT_{w-c} with Time.

Figure 4. Distribution of Ambient Temperature (T_a), Glass Cover Temperature (T_c), Absorber Plate Temperature (T_p), and Basin Water Temperature with Time (ΔT_{w-c}): (a) SS System; (b) STC System; (c) SS+STC System; and (d) Variation of ΔT_{w-c} with Time.

proach to predict the thermal performance of the system. However, the observed deviations may be attributed to measurement uncertainty, sensor positioning during data acquisition, partial shading at the experimental site, and short-term cloud fluctuations during the measurement period.

3.2. Thermal Response of the System: Distribution of Ambient Temperature (T_a), Glass Cover Temperature (T_c), Absorber Plate Temperature (T_p), and Basin Water Temperature

Important factors affecting the performance of the solar still (SS) and solar thermal collector (STC) systems include the distributions of ambient temperature, glass cover temperature, absorber plate temperature, and basin water temperature. These temperatures play a crucial role in determining the performance of the solar still and solar thermal collector systems, as temperature is a key parameter governing heat transfer, mass flow rate, evaporation rate, and system thermal efficiency. The analytical calculation results for ambient temperature, glass cover temperature, absorber plate temperature, and basin water temperature as functions of time are presented in Figure 4.

Based on Figure 4, the SS system showed an average ambient temperature of 31.54°C, an average absorber plate temperature of 48.5°C, an average glass cover temperature of 38.27°C, an average basin water temperature of 41.76°C, and an average temperature difference ΔT_{w-c} of 3.49°C. In the solar still system, the absorber plate temperature was higher than the glass cover and ambient temperatures. This occurs because the absorber plate directly receives solar radiation and acts as the primary heat absorbing surface. The absorbed heat is then transferred to the basin water, thereby increasing the water temperature and promoting the evaporation process. The temperature of the absorber plate was higher than that of the glass cover because the glass not only receives heat from vapor and internal radiation but also releases heat to

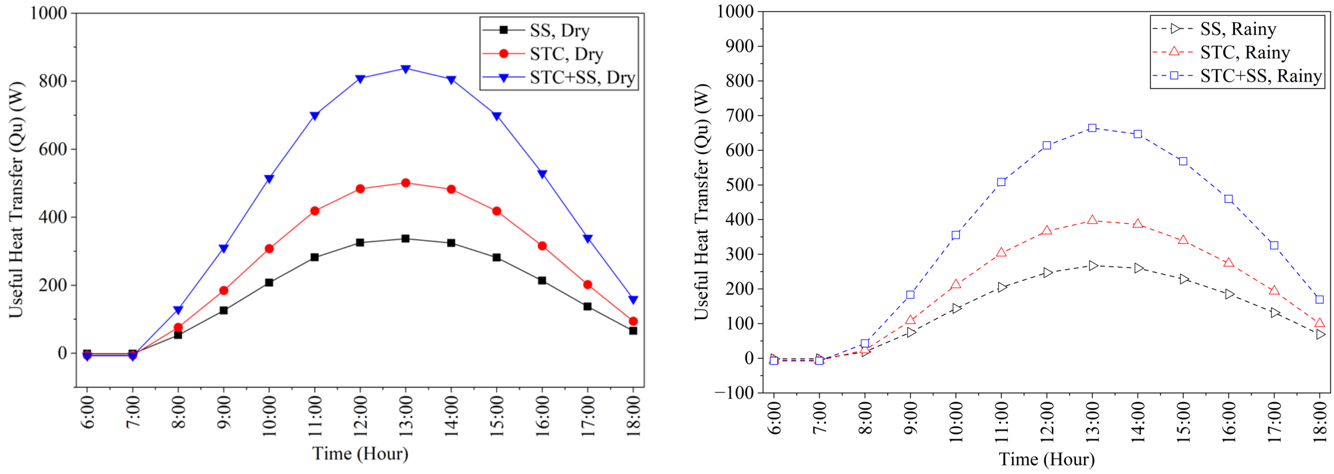

(a) Dry Season **(b)** Rainy Season

Figure 5. Distribution of Useful Heat Gain (Q_u) of the Solar Water Distillation System with Time under Two Different Seasons: (a) Dry Season and (b) Rainy Season.

the environment through convection and radiation. This condition is required because the condensation process needs a glass surface that is relatively cooler than the water vapor inside the solar still chamber.

In the STC system, the average ambient temperature, absorber plate temperature, and glass cover temperature were 31.54°C, 63.04°C, and 50.93°C, respectively. These results indicate that the absorber plate temperature was considerably higher than that of the SS system, as the collector maximizes solar radiation absorption and transfers heat to the air. The high absorber temperature indicates that the system is capable of significantly absorbing and storing solar radiation energy. An increase in T_p can enhance the evaporation rate and distillate productivity. This finding is consistent with the study by Aghakhani et al. (2023), which reported that an increase in T_p leads to higher evaporation energy, as the latent heat required for water evaporation can be supplied more rapidly at elevated temperatures [18].

In the SS+STC system, the average ambient temperature, absorber plate temperature, glass cover temperature, and basin water temperature were 31.54°C, 65.46°C, 59.42°C, and 61.77°C, respectively, with an average temperature difference ΔT_{w-c} of 2.35°C. The temperature difference between the basin water and the glass cover is an important parameter because it acts as the driving force for evaporation and condensation. As the water temperature increases, the saturated vapor pressure rises, resulting in more intensive evaporation [19]. However, condensation still requires a lower glass cover temperature so that the vapor can be converted into distillate. In the SS+STC system, the additional heat supply from the collector increases the basin water temperature, thereby intensifying the evaporation process. However, if the glass cover temperature becomes too high, the condensation effectiveness may decrease because the temperature gradient between the vapor and the glass surface becomes smaller. The condensation mechanism in a solar still begins when incident solar radiation enters the system and is absorbed by the absorber surface, resulting in an increase in the temperature of the saline water. As the water temperature rises, evaporation occurs, generating water vapor within the enclosed chamber. Condensation subsequently takes place on the inner surface of the transparent glass cover, where the vapor comes into contact with a surface temperature lower than its dew point. Under these conditions, the saturated water vapor releases its latent heat to the glass surface and undergoes a phase transition into liquid droplets. These condensate droplets gradually flow along the inclined glass surface and are collected through the distillate channel as purified water.

Conversely, when the glass temperature approaches the vapor temperature, both the temperature gradient and the vapor pressure difference between the evaporating water surface and the condensing glass decrease. This reduction weakens the driving force for heat and mass transfer, leading to a lower condensation rate and reduced freshwater productivity. This phenomenon is consistent with the dew-point theory, which states that condensation occurs when moist air or water vapor reaches saturation and comes into contact with a surface whose temperature is lower than the dew-point temperature, causing the vapor to undergo a phase change into liquid water.

3.3. Useful Energy Gain and Thermal Efficiency of the SS, STC, and SS+STC Systems

The distribution of useful energy gain (Q_u) represents the amount of thermal energy absorbed by the working fluid to increase the outlet fluid temperature. In this study, analytical calculations were performed to determine the useful energy gain (Q_u) in the SS, STC, and integrated SS+STC systems. The magnitude of useful heat gain (Q_u) is influenced by the absorbed solar radiation (S) and is

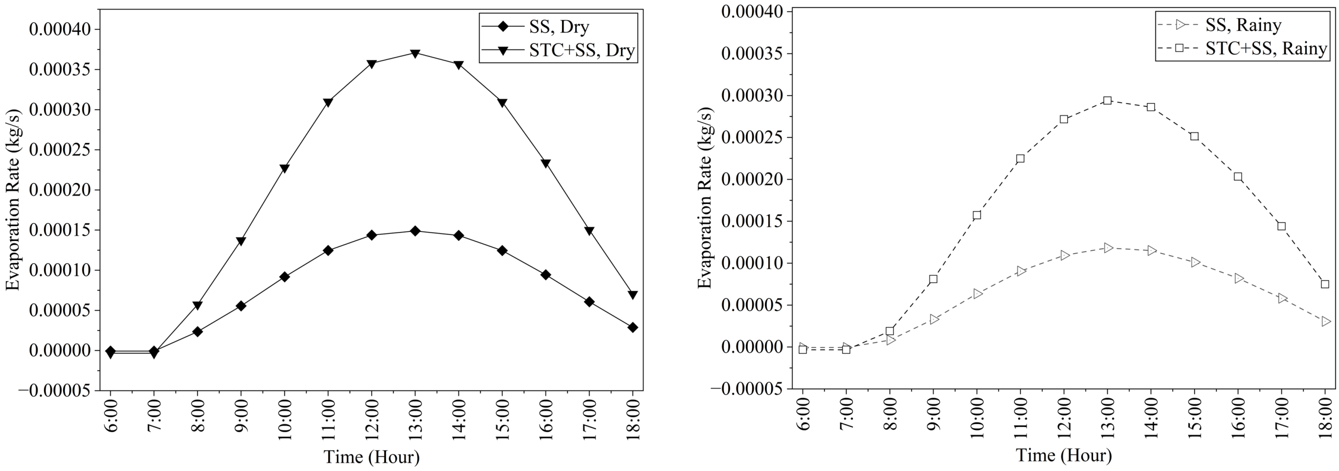

(a) Dry Season **(b)** Rainy Season

Figure 6. Evaporation Rate of the SS and SS+STC System with Time under Two Different Seasons: (a) Dry Season and (b) Rainy Season.

inversely affected by the thermal heat losses of the system, expressed as $S - U_L(T_{pm} - T_a)$. As the solar radiation intensity increases during the daytime, the absorbed solar radiation also increases, resulting in a higher useful heat transfer rate. The useful heat gain (Q_u) was analyzed for the solar still (SS), solar thermal collector (STC), and the integrated solar still with solar thermal collector (SS+STC) systems. The distribution of useful energy gain (Q_u) as a function of time is presented in Figure 5.

Based on Figure 5(a), the analytical calculation results of useful heat gain (Q_u) during the dry season are presented. For the solar still (SS) system, the maximum Q_u value was 336.9 W at 13:00 WIB. This relatively low value indicates that the conventional system relies only on direct heat absorption in the basin without additional integration with an STC. The addition of the STC provides a significant increase in useful heat gain. For the STC system, the maximum Q_u value was 501.39 W. The increase in Q_u indicates that the STC is capable of enhancing solar radiation absorption and increasing the thermal energy transferred to the basin water. Consequently, the integrated SS+STC system produced the highest maximum Q_u value, reaching 838.29 W. This result indicates that the integrated system can increase the accumulation of absorbed thermal energy, thereby providing greater useful heat for the evaporation process.

Based on Figure 5(b), the analytical calculation results of useful heat gain (Q_u) during the rainy season are presented. For the solar still (SS) system, the lowest Q_u value was obtained, with a maximum value of 267.34 W at 13:00 WIB. This low value indicates that the conventional SS system depends only on direct heat absorption in the basin without additional integration with an STC. The addition of the STC significantly improves the useful heat gain. For the STC system, the maximum Q_u value was 397.05 W. Although the Q_u value decreased compared with that in the dry season, the STC was still able to enhance solar radiation absorption and increase the thermal energy transferred to the basin water. Therefore, the integrated SS+STC system produced the highest maximum Q_u value, reaching 664.39 W.

These results indicate that the solar still (SS) integrated with a solar thermal collector (STC) has a higher Q_u distribution than the SS system without STC integration. This is because the addition of the STC increases the thermal energy gain from solar radiation, resulting in greater heat acquisition compared with the system without an STC. As a result, the Q_u of the SS+STC system becomes higher than that of the standalone SS system. In general, higher solar radiation intensity leads to greater thermal energy absorption by the working fluid. The thermal efficiency performance of the solar water distillation system was evaluated as a function of time for three system configurations: the solar still (SS), the solar thermal collector (STC), and the integrated SS+STC system.

The useful heat gain (Q_u) plays a critical role in enhancing the thermal performance of the desalination system by increasing both the absorber plate temperature (T_p) and the water temperature (T_w). An increase in Q_u provides additional thermal energy for sensible heating and accelerates the evaporation process, thereby increasing the quantity of water vapor generated inside the solar still. Efficient condensation occurs when the glass cover temperature (T_c) remains below the dew-point temperature of the water vapor. Under this condition, the vapor transfers its latent heat to the cooler glass surface and condenses into distillate droplets.

Based on Figure 6, the evaporation rate of the solar water distillation system shows significant changes over time from 06:00 to 18:00 WIB during both the dry and rainy seasons. The graph also indicates that after 13:00 to 14:00 WIB, the evaporation rate of all systems begins

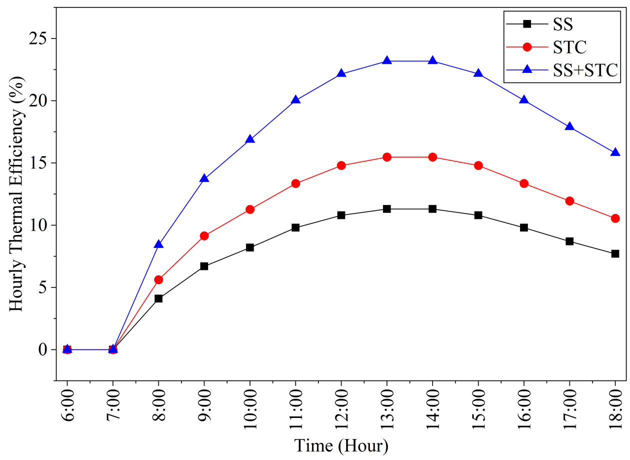

Figure 7. Thermal Efficiency of the SS, STC, and SS+STC Systems as a Function of Time.

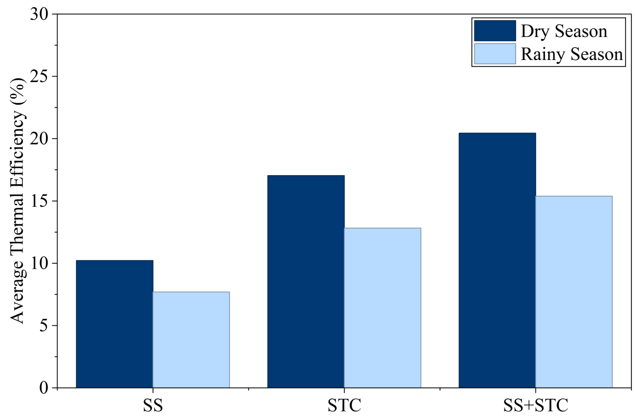

Figure 8. Daily average thermal efficiency of the SS, STC, and SS+STC systems under dry and rainy season conditions.

to decrease. This condition occurs because the intensity of solar radiation starts to decline in the afternoon, resulting in a reduction in the thermal energy received by the system. The decrease in absorber and water temperatures gradually reduces the rate of water vapor formation. Nevertheless, the integration of the solar thermal collector (STC) with the solar still (SS) is able to maintain a higher evaporation rate than the conventional SS until the end of the testing period. This indicates that the thermal collector has a better ability to retain and supply accumulated heat to the system.

Figure 6(a) shows the evaporation rate of the SS system and the integrated SS-STC system during the dry season. In the dry season, the SS system produces an evaporation rate of 0.000149 kg/s, while the maximum evaporation rate of the integrated SS-STC system reaches 0.00037 kg/s. Therefore, the SS-STC system produces the highest evaporation rate compared with the conventional SS system. This difference indicates that the addition of the STC is able to increase the thermal energy supply to the SS system, resulting in a higher basin water temperature. Consequently, the amount of evaporated water in the integrated SS-STC system is greater than that in the SS system without STC integration.

Figure 6(b) shows the evaporation rate of the solar water distillation system over time during the rainy season. Under rainy-season conditions, the increasing and decreasing trends of the evaporation rate show a similar pattern to those observed during the dry season. However, the overall evaporation rate is lower than that in the dry season. The SS-STC system during the rainy season produces a maximum evaporation rate of approximately 0.00029 kg/s, while the SS system during the rainy season reaches only about 0.00012 kg/s. This decrease in performance is influenced by the lower intensity of solar radiation due to cloud cover and higher air humidity during the rainy season. These conditions reduce the amount of thermal energy absorbed by the absorber, causing the increase in basin water temperature to be lower than that during the dry season. In addition, the lower ambient temperature also reduces the driving force for heat and mass transfer during the evaporation process. As the operating time increases, the solar radiation received by the absorber also increases, causing the basin water temperature to rise and accelerating the evaporation process. Overall, the integrated SS-STC system demonstrates better thermal performance than the conventional SS system because the additional heat supplied by the solar thermal collector enhances the evaporation rate, particularly during periods of high solar radiation intensity. The thermal efficiency profiles of the SS, STC, and SS+STC systems with time are shown in Figure 7.

Based on Figure 7, the thermal efficiency of the three system configurations shows an increasing trend from morning to midday, followed by a decrease in the afternoon. The solar still (SS) system exhibited the lowest efficiency compared with the other configurations, with a maximum efficiency of 11.3% and a daily average efficiency of 9.02%. The solar thermal collector (STC) system showed higher efficiency, with a maximum efficiency of 15.48% and an average efficiency of 12.34%. Meanwhile, the integrated SS+STC system achieved the highest efficiency, with a maximum efficiency of 23.19% and a daily average efficiency of 18.5%. These results indicate that the addition of a solar thermal collector can significantly improve the thermal performance of the solar still system.

Based on Figure 8, the efficiency improvement resulting from the addition of the STC can be observed from the efficiency difference between the SS and SS+STC systems. Based on the data, the maximum efficiency increased from 10.22% in the SS system to 20.44% in the SS+STC system during the dry season. Meanwhile, during the rainy season, the daily average thermal efficiency increased from 7.69% in the SS system to 15.39% in the SS+STC system.

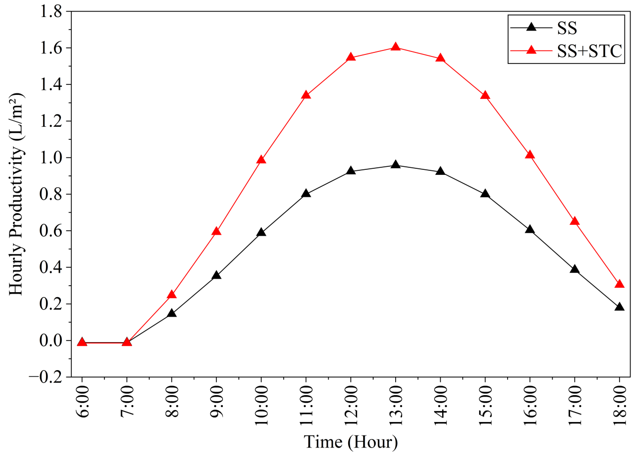

Figure 9. Hourly distillate productivity of the SS and SS+STC systems.

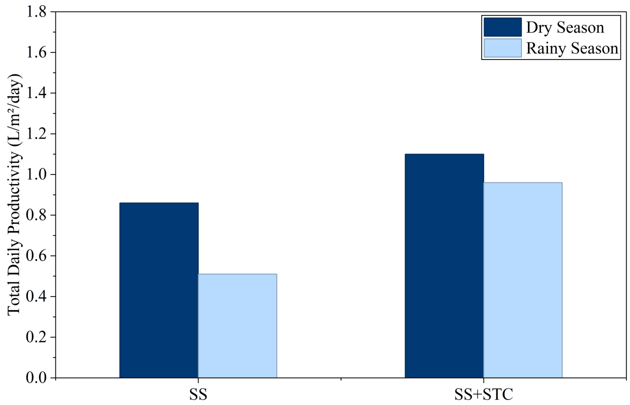

Figure 10. Daily average distillate productivity of the SS and SS+STC systems under dry and rainy season conditions.

Table 4. Daily average thermal efficiency of the analyzed configurations.

Season	SS (%)	STC (%)	SS+STC (%)
Dry Season	10.22	17.04	20.44
Rainy Season	7.69	12.82	15.39

Table 5. Daily distillate productivity.

Season	SS ($L/m^2/day$)	SS+STC ($L/m^2/day$)
Dry Season	0.86	1.10
Rainy Season	0.51	0.96

These values indicate that STC integration not only improves instantaneous efficiency under maximum radiation conditions but also enhances the overall daily thermal performance of the system. The improvement in efficiency in the SS+STC system occurs due to the additional thermal energy supplied by the collector.

In the SS system, heat energy in the SS system comes solely from solar radiation that the absorber plate and basin directly receive. A portion of this energy is utilized to heat the water in the basin, while the rest is lost to the surroundings through convection, thermal radiation, the glass cover, the side walls, and the basin bottom. In the SS+STC system, solar radiation is not only utilized by the solar still but is also collected by the STC to heat the air, which is subsequently directed into the evaporation chamber. This heated air carries additional thermal energy to the basin water, thereby increasing the useful heat gain (Q_u) and accelerating the evaporation process.

3.4. Distillate Water Productivity, System Comparison, and Design Implications

An analytical study was conducted to analyze heat transfer and evaluate the performance of the solar thermal collector and solar still systems. The research was carried out using an analytical method based on a research-variable matrix consisting of a solar still (SS), a solar thermal collector (STC), and an integrated SS+STC system. The calculations were performed using weather data, including solar radiation intensity and ambient temperature. The productivity of the solar water distillation system as a function of time is shown in Figure 9.

Based on Figure 9, the evolution of solar water distillation productivity with time shows that both the system without STC integration (SS) and the system with STC addition exhibit an increasing productivity trend as solar radiation intensity rises from morning to midday, followed by a decrease in the afternoon. The highest productivity was achieved between 12:00 and 13:00 WIB, indicating that the evaporation and condensation processes occurred most optimally when solar radiation intensity reached its maximum value. Distillate water productivity was analyzed in terms of hourly productivity and daily productivity to compare the performance of the conventional SS system with that of the SS system integrated with an STC.

In the SS system, water productivity began to increase at 09:00 WIB and reached a maximum value of approximately 0.958 L/m^2 at 13:00 WIB. After reaching the peak condition, productivity gradually decreased to approximately 0.179 L/m^2 at 18:00 WIB due to the decrease in solar radiation intensity and basin water temperature. As solar radiation intensity increased, the absorber temperature and basin water temperature also increased, thereby enhancing the evaporation rate. Meanwhile, the SS+STC system showed higher distillate water productivity than the conventional SS system over almost the entire observation period. The integration of the solar thermal collector increased the amount of thermal energy absorbed by the system, allowing the basin water temperature to rise more rapidly and be maintained for a longer period. This condition intensified the evaporation process.

Based on the research results shown in Figure 10, the daily average productivity of the SS+STC system was higher than that of the conventional SS system under both seasonal conditions. During the dry season, productivity increased from 0.86 L/m^2/day to 1.10 L/m^2/day, whereas during the rainy season, it increased from 0.51 L/m^2/day to 0.96 L/m^2/day. This improvement indicates that the addition of a solar thermal collector (STC) can increase the heat input to the basin, thereby increasing the water temperature and intensifying the evaporation process. These results demonstrate that the use of an external solar collector can increase the saline water temperature and produce higher distillate water productivity compared with a conventional solar still. This improvement occurs because the collector provides additional thermal energy that accelerates the evaporation process inside the basin.

In addition to the effect of system configuration, seasonal variation also has a significant impact on productivity. During the dry season, higher solar radiation intensity increases the energy absorbed by the absorber, allowing the basin water temperature to reach higher values. Therefore, the productivity of the integrated SS+STC system reached 1.10 L/m^2/day, whereas during the rainy season it decreased to 0.96 L/m^2/day. This reduction occurred due to the lower solar radiation received by the collector and basin, which was caused by higher cloud cover and shorter sunshine duration.

Although the SS+STC system improves useful heat gain, thermal efficiency, and distillate productivity, its performance remains dependent on solar radiation intensity and ambient conditions. Under cloudy or rainy conditions, the heat supplied by the collector decreases, reducing the basin water temperature and evaporation rate. In addition, excessive glass cover temperature may reduce the water–glass temperature difference, which can weaken the condensation process. Therefore, future improvements may include glass cover cooling, improved insulation, optimized airflow rate, and collector geometry optimization.

4. Conclusions

This study analytically evaluated the performance of a solar still integrated with a solar thermal collector under dry and rainy season conditions. With MAPE values less than 3.37%, the analytical model demonstrated strong agreement with experimental data. The results show that the SS+STC configuration provides better performance than the conventional SS system by increasing useful heat gain, thermal efficiency, and distillate productivity. The daily average thermal efficiency increased from 10.22% to 20.44% in the dry season and from 7.69% to 15.39% in the rainy season. In addition, daily productivity increased from 0.86 to 1.10 L/m^2/day during the dry season and from 0.51 to 0.96 L/m^2/day during the rainy season. Overall, integrating a solar thermal collector is an effective approach to enhance the thermal performance and freshwater productivity of a solar still, although system performance remains strongly influenced by seasonal solar radiation intensity.

Acknowledgments

The authors acknowledge the Department of Engineering Physics, Institut Teknologi Sepuluh Nopember, for academic and laboratory support during the development of this study. The authors also thank the thesis supervisors and examiners for their technical suggestions during the research process.

References

[1] H. Xu and H. Luo, "Breakthroughs and prospects: The development path of solar thermal seawater desalination technology," in *Environmental Sciences*, London, UK: IntechOpen, Feb. 2025.

[2] F. A. Essa, A. Abdullah, H. S. Majdi, B. Al-Waeli, H. A. Dhahad, Z. M. Omara, S. A. Mohammed, W. H. Alawee, A. A. Ezzi, and T. Yusaf, "Parameters affecting the efficiency of solar stills—recent review," *Sustainability*, vol. 14, no. 17, p. 10668, 2022.

[3] R. H. Mohammed and A. A. Askalany, "Solar desalination technology," in *Green Energy and Technology*, pp. 325–357, Singapore: Springer, 2019.

[4] M. M. Mekonnen and A. Y. Hoekstra, "Four billion people facing severe water scarcity," *Science Advances*, vol. 2, p. e1500323, Feb. 2016.

[5] R. Bhardwaj, M. V. ten Kortenaar, and R. F. Mudde, "Influence of condensation surface on solar distillation," *Desalination*, vol. 326, pp. 37–45, Oct. 2013.

[6] H. M. Qiblawey and F. Banat, "Solar thermal desalination technologies," *Desalination*, vol. 220, no. 1–3, pp. 633–644, 2008.

[7] D. Marghade, G. Mehta, S. Shelare, G. Jadhav, and K. C. Nikam, "Arsenic contamination in indian groundwater: From origin to mitigation approaches for a sustainable future," *Water*, vol. 15, no. 23, p. 4125, 2023.

[8] M. A. Tony and H. A. Nabwey, “Recent advances in solar still technology for solar water desalination,” *Applied Water Science*, vol. 14, p. 147, July 2024.

[9] J. Feria-Díaz, M. López-Méndez, J. Rodríguez-Miranda, L. Sandoval-Herazo, and F. Correa-Mahecha, “Commercial thermal technologies for desalination of water from renewable energies: A state-of-the-art review,” *Processes*, vol. 9, p. 262, Jan. 2021.

[10] G. N. Tiwari and L. Sahota, *Advanced Solar-Distillation Systems*. Green Energy and Technology, Singapore: Springer, 2017.

[11] E. A. Ashour, “Use of agriculture-based waste for basic dye sorption from aqueous solution: Kinetics and isotherm studies,” *American Journal of Chemical Engineering*, vol. 2, no. 6, pp. 92–98, 2014.

[12] F. M. Abed, M. H. Zaidan, M. Hasanuzzaman, L. Kumar, and A. K. Jasim, “Modelling and experimental performance investigation of a transpired solar collector and underground heat exchanger assisted hybrid evaporative cooling system,” *Journal of Building Engineering*, vol. 44, p. 102620, 2021.

[13] V. D. Naidu, “Performance evaluation of an enhanced solar still using simulink,” *Journal of Electrical Systems*, vol. 20, no. 5s, pp. 1204–1216, 2024.

[14] H. Hassan, “Comparing the performance of passive and active double and single slope solar stills incorporated with parabolic trough collector via energy, exergy and productivity,” *Renewable Energy*, vol. 148, pp. 437–450, Apr. 2020.

[15] B. S. S. Wibawa, Y. C. Wang, G. Andhikaputra, Y. K. Lin, L. H. C. Hsieh, and K. H. Tsai, “The impact of climate variability on dengue fever risk in central java, indonesia,” *Climate Services*, vol. 33, p. 100433, Jan. 2024.

[16] J. A. Duffie, W. A. Beckman, and N. Blair, *Solar Engineering of Thermal Processes, Photovoltaics and Wind*. Hoboken, NJ: John Wiley & Sons, 5 ed., 2020.

[17] T. L. Bergman, A. S. Lavine, F. P. Incropera, and D. P. DeWitt, *Fundamentals of Heat and Mass Transfer*. John Wiley & Sons, 7 ed., 2011.

[18] H. Aghakhani, S. M. Ayatollahi, and M. R. Hajmohammadi, “Proposing novel approaches for solar still performance enhancement by basin water heating, glass cooling, and vacuum creation,” *Desalination*, vol. 567, p. 117011, Dec. 2023.

[19] A. P. Singh, A. Kumar, Akshayveer, and O. P. Singh, “Natural convection solar air heater: Bell-mouth integrated converging channel for high flow applications,” *Building and Environment*, vol. 187, p. 107367, Jan. 2021.